NJC

Accepted Manuscript

This is an *Accepted Manuscript*, which has been through the Royal Society of Chemistry peer review process and has been accepted for publication.

Accepted Manuscripts are published online shortly after acceptance, before technical editing, formatting and proof reading. Using this free service, authors can make their results available to the community, in citable form, before we publish the edited article. We will replace this *Accepted Manuscript* with the edited and formatted *Advance Article* as soon as it is available.

You can find more information about *Accepted Manuscripts* in the Information for Authors.

Please note that technical editing may introduce minor changes to the text and/or graphics, which may alter content. The journal's standard Terms & Conditions and the Ethical guidelines still apply. In no event shall the Royal Society of Chemistry be held responsible for any errors or omissions in this *Accepted Manuscript* or any consequences arising from the use of any information it contains.

ROYAL SOCIETY OF CHEMISTRY

www.rsc.org/njc

Generation of Highly Ordered Nanoporous Sb-SnO_2 Thin Films with Enhanced Ethanol Sensing Performance at Low Temperature

Shaofeng Shao [a,*], Ralf Koehn[b], Hongyan Wu[a], Tao Wu[a], Wei-Feng Rao [a]

[a]*Department of Materials Physics, School of Physics and Optoelectronic Engineering, Nanjing University of Information Science &Technology, Nanjing, China.*

[b]*Department of Chemistry & Biochemistry, University of Munich, Munich, Germany.*

** Corresponding author. Fax: +86-025-58731031; Tel: +86-025-58731031;*

E-mail address: ssfshao@nuist.edu.cn (Shaofeng Shao)

Abstract

Highly ordered nanoporous Sb-doped tin dioxide (Sb-SnO_2) thin films are crystallized by a 120°C post-synthetic hydrothermal treatment for gas sensing applications. The resulted thin films can be annealed, as desired, at temperatures up to 600°C for removing the templates and tuning the sensitivities without destroying the nanostructures. It is found that Sb-SnO_2 films doped with 8wt% Sb can well satisfy the demands for high gas sensitivity at low operation temperature, e.g., a change of ~30 times of electric resistance in response to 50 ppm ethanol is rapidly detected at temperature as low as 100°C. The structure, crystallinity, and composition of the ordered nanoporous Sb-SnO_2 thin films are characterized by HRTEM, FESEM, SAED, and STEM. The developed synthesis method represents a flexible route generally applicable for preparing nanoporous metal oxide crystalline films for applications including gas sensing, photocatalysis, and 3rd generation photovoltaics.

Keywords: Tin dioxide; antimony doping; nanoporous thin films; spin-coating; ethanol gas sensor

1. Introduction

Gas sensors have been intensively investigated in recent years due to their fundamental scientific interest and technological applications such as air-quality control, environmental monitoring, healthcare, defence and security, and other applications. [1-6] The performance of gas sensors is primarily determined by the properties of sensing materials and their nanostructures because these factors strongly affect the interactions between the analyzed molecules and the surface of the sensing materials, and the subsequent generation of output signals. [7-9] Recent developments in nanotechnologies have made available a variety of nanostructured sensing materials with increased surface-to-volume ratios, which effectively offers large contact area to the environment for promptly and reliably detecting a broad range of gases in low concentrations with high rate, sensitivity, selectivity, and reversibility. [10-15]

In principle, ordered nanoporous films of sensing materials offering large surface-to-volume ratios and highly sensitive electric properties should allow sensitive transduction of the gas/surface interactions into a change of the electrical conductivity [16-19], which is therefore of great interest for the development on promising platform for the next generation sensor materials [20]. However, nanoporous gas sensing materials synthesized by conventional methods, *e.g.* sol-gel, generally suffer a significant decrease in effective surface area due to the nanostructure collapse during the annealing process at high temperature (>250°C) [21, 22]. In addition, to activate the reaction of oxygen chemisorptions and surface catalysis, gas sensors based on conventional materials generally require a high operation temperature for achieving a measureable gas response. This thus partly explain that, although the nanoporous thin film-based sensors have been studied world-wide, gas sensors that can quickly detect target gases at low-level concentration at low operated temperature are still in a demand [23].

In order to increase the sensitivity and reliability of the sensing materials, it is highly desired to fabricate nanoporous thin films of sensitive materials that are thermally more stable. Besides, the size, arrangement, and surface doping of ordered nanoporous thin films should also be optimized for better properties at low operation temperature. If the radius of ordered porous nanostructures can be close to

the material's Debye length, such porous architecture can greatly impact mobile charge carriers concentration in response to surface redox process [24]. The facile charge transfer property is beneficial to establish an extreme sensitivity of the electron transport to charge transfer interactions of gas molecules at the surface of material [25-27]. Therefore, highly ordered nanoporous structure with small crystal particle sizes and excellent particle interconnectivity are desired for manufacturing high performance gas sensors to be used at low temperature.

SnO_2 based materials are promising candidates for fabricating nanoporous thin films to be used in gas sensors because they are highly sensitive to various toxic and flammable gases including CH_4, H_2, CO, H_2S, and NO_x.[28, 29] Besides, SnO_2 is of low cost, high response speed, high stability, and low power consumption[30-33]. By proper doping noble metals, the sensing properties of SnO_2 based thin films can be dramatically improved in terms of selectivity and long-term stability[34-38]. Compared with noble metals, antimony is a common n-type dopant. Much research work for the synthesis and preparation of antimony doped SnO_2 are concentrated on the use of these materials in transparent electrodes, catalysts, photovoltaic devices, and energy-storage devices. However, there is few report on the sensing performance of Sb doped SnO_2 nanoporous thin films to VOCs at low temperature. Antimony can be used to improve the sensing performance because (1) Sb doping can increase the charge carrier concentration of SnO_2 film and thus facilitate the electron transfer during the interaction with target gases, and (2) consequently, the generation of a large amount of oxygen vacancies and chemisorbed oxygen species can lead to sensing response enhancement. Therefore, highly ordered nanoporous Sb-doped SnO_2 thin films are synthesized and characterized, and the gas (ethanol) sensing property of the obtained films are examined in this paper.

A effective method to fabricate nanostructured thin films of tin dioxide with long-range ordered nanostructure was introduced by Miyata and co-workers [39]. A post-synthesis water vapour treatment was employed to synthesize highly ordered nanostructured tin oxide thin films. After subjecting the films to water vapour at 70°C, a disorder-to-order phase transition took place, leading to the formation of ordered nanostructures. However, annealing of the nanoporous thin films for removal of the surfactant templates commonly results in a phase change and collapse of the porous structure up to 600 °C [40, 41]. Based on the above mentioned methods we developed a post synthetic hydrothermal treatment for the synthesis of highly ordered nanoporous Sb-SnO_2 sensing films. Briefly, an ethanolic solution containing a tin oxide precursor and dopant as well as an organic template is spin-coated onto a sensor device. Upon the treatment, the system co-assembles to form an inorganic/organic composite with nanoscale periodicity and crystalline nanoparticles. This composite is then thermally treated to remove the organic template and to further increase crystallinity of pore walls. The structure, crystallinity and composition of the ordered nanoporous Sb-SnO_2 thin films are characterized by HRTEM, FESEM, SAED, and STEM.

2. Experimental details

2.1 Sensing Film Fabrication and Characterizations.

The Sn precursor solutions were prepared by dissolving 1 g $SnCl_4$ (Aldrich) in 7.0463 g ethanol in the presence of 0.4836 g PluronicF127 triblock copolymer ($[(HO(CH_2CH_2O)_{106}-(CH_2CH(CH_3)O)_{70}-(CH_2CH_2O)_{106}H$, $EO_{106}PO_{70}EO_{106}]$, Sigma). For Sb doping, 0.08 g $SbCl_3$ (Aldrich) was dissolved in 1.92 ml 12 M HCl and then mixed with the above tin precursor solution under constant stirring for 12 h. The resulting (clear) Sb-Sn precursor solutions were stable over a two-week period. The molar ratio of $SnCl_4$:F127:EtOH:$SbCl_3$:HCl:H_2O in the final Sb-Sn precursor solution was 1:0.01:40:0.0914:6:21.

Gas sensing thin films were prepared by spin-coating 50 µl of the Sb-Sn precursor solution onto an interdigital electrode at 4000 rpm for 90 s under 10% relative humidity for five times, and then dried at 60°C for 2 h. The films were then exposed to a water vapour hydrothermal treatment, 95% relative humidity, at 120°C for 12 h. The relative humidity was achieved using a supersaturated $CuSO_4$ aqueous solution, kept at 120°C, in a closed chamber. The organic surfactant templates were then removed by annealing at temperatures of 400°C for 1 h, or 600°C for 1 h, with an up/down ramp rate of 1.0°C/min.

SAXRD patterns of the thin films were taken on an XDS-2000 diffractometer (Scintag Inc.) using Cu K radiation. WAXRD data were obtained by a Bruker D8 Advance X-ray diffractometer with Cu Ka (0.15406 nm) radiation. Field-emission scanning electron microscopy (FE-SEM, Hitachi S-4800) was used to observe the morphologies of the sensing films. Nitrogen sorption measurements were carried out at 77 K using a NOVA 4000e (Quantachrome Instruments) on Sb doped tin oxides scratched from several films. High resolution transmission electron microscopy (HRTEM) and scanning transmission electron microscopy in high angle annular dark field mode (STEM-HAADF) were performed using a FEI Titan 80-300 equipped with a field emission gun operated at 300 kV; film parts were scratched from the substrate and collected on an amorphous holey carbon film on a copper grid. XPS spectra were recorded using a Kratos Axis Ultra DLD spectrometer employing a monochromated Al-Ka X-ray source (hv= 1486.6 eV), hybrid (magnetic/electrostatic) optics and a multi-channel plate and delay line detector (DLD). Surface charging was corrected by referencing the spectra to C-C state of the C 1s peak at binding energy at 284.6 eV. All XPS spectra were recorded using an aperture slot of 300*700 microns, survey spectra were recorded with a pass energy of 160 eV, and high resolution spectra with a pass energy of 40 eV.

2.2 Gas-Sensing Measurement

During the sensing measurement, liquid VOCs were inputted through a sample inlet and led down to a heater, which vaporized it. A fan ensured that the vapour was homogeneously distributed. The gas sensing properties were determined in a sample cell consists of a sample chamber and has a gas inlet and outlet. Resistance changes upon sample exposure to gases were recorded by a high resistance meter Keithley 6517A. The sensor response is defined as $S= (R_a-R_g)/R_g$ or= $(R_g-R_a)/R_a$, where R_a and R_g are the sensor resistances in air and in the target gas, respectively. Here, the response or recovery time is defined as the time taken for the sensor to achieve 90% of its maximum response or decreases to 10% of its maximum response, respectively.

3. Results and discussion

3.1 Material Properties

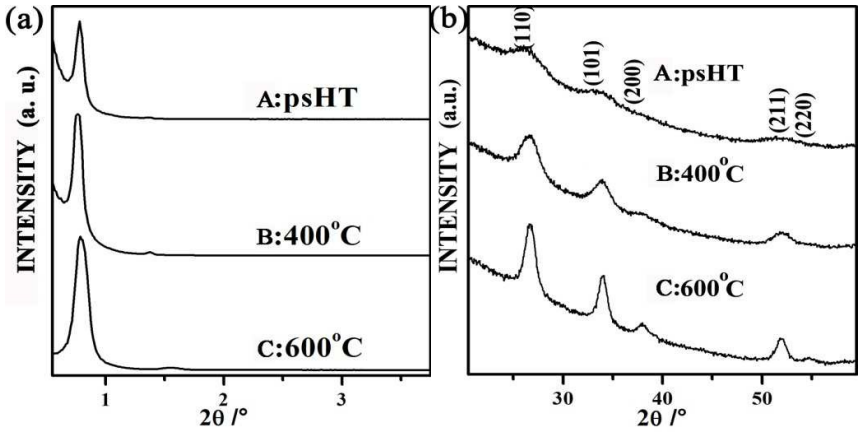

Fig. 1. (a) Small-angle XRD patterns of nanoporous 8wt% Sb-SnO_2 thin films synthesized after: (A) 120°C hydrothermal treatment; annealing at (B) 400°C and (C) 600°C. (b) XRD patterns of nanoporous 8wt% Sb-SnO_2 thin films after: (A) 120°C hydrothermal treatment; annealing at (B) 400°C and (C) 600°C.

The crystallinity and structure of the synthesized thin films were examined by X-ray diffraction (XRD, Scintag, Inc. XDS-2000, Cu Kα radiation). For the as-synthesized air-dried Sb-SnO_2 thin films, no diffraction peaks were observed within the small angle XRD (SAXRD) patterns (not shown for brevity), indicating a disordered nanostructure. An ordered nanostructure formed after exposing the Sb-SnO_2 thin films to the hydrothermal treatment (120°C, 12 h) was indicated by the peak appearing at ≈ 0.59° on the SAXRD pattern, Fig. 1a. Doping levels during the synthetic procedure have been proved to have significant influence in the nanstructure ordering during the the fabrication of nanoporous metal oxides. In this work, the one main research aim is to find the particular relation between the nanostructured ordering of nanoporous Sb doped SnO_2 sensing films and their gas sensing property. For this purpose, the SAXRD patterns of the thin films of SnO_2 doped with different concentration of Sb are depicted in ESI, Fig. S1: 2wt%, 4wt%, 6wt%, 8wt% and 10wt%, respectively. All five films treated by hydrothermal treatment exhibit an ordered nanostructure. The ordered nanostructure of the thin film is then retained through the progressive thermal treatment. After calcination at 400°C, as the concentration of Sb increases from 2wt% to 8wt%, the diffraction peaks become sharper and stronger, and then the diffraction peak intensity decreases with further increase in the Sb concentration. The decrease of peak intensity can be interpreted as a reduction in the X-ray diffraction contrast between the pore and the framework, indicating that the nanostructured ordering of SnO_2 can be varied by the change of Sb concentrations. Compared with the post-synthetic hydrothermal treated films, the 400°C annealed sensing films with 8wt% Sb show a considerably stronger and sharper peak. As a result, 8wt% of Sb is optimal content of dopant for obtaining highly ordered nanoporous structure of SnO_2 thin film. Ellipsometric measurements indicated a film thickness of ≈ 891 nm. The small-angle XRD patterns of the nanoporous SnO_2 thin film heat-treated at 600°C is illustrated in Fig. 1a. The pattern of the calcined sample still reveals a sharp and strong peak at each calcination temperature, showing that the highly ordered nanostructure is preserved up to 600°C. The peak position shifts to 0.63° for the 400°C film, and 0.69° for the 600°C film as the thickness of the film decreases slightly, to ≈ 849 nm for the 400°C annealed film and ≈ 789 nm for the 600°C annealed film. As shown in ESI, Fig. S2, the Grazing-Incidence Small-Angle X-ray Scattering (GISAXS) pattern of the Sb-SnO_2 thin films exhibit a behavior assigned to a highly ordered nanostructure with F*mmm* orthorhombic symmetry.Compared with the hydrothermally treated thin film, the pattern of the 600°C annealed film is stronger, indicating the excellent thermal stability of the ordered nanoporous structure. Since ordered nanoporous

topologies are known to commonly collapse with annealing at temperatures as low as 250°C, the described synthesis technique represents a significant advance in the ability to maintain the high temperature structural stability of such highly ordered nanoporous architectures. The above results indicate that the described synthesis technique is a versatile means to create well-defined nanopores with narrow pore-size distribution and high specific surface areas, and makes it possible to prevent undesired changes in the pore structure upon high-temperature treatment. Such treatment plays a vital role in improving the material's nanostructure, long-term thermal stability and gas-sensing property.

As suggested by Tiemann [14], an ideal gas sensing layer should have a grain size up to approximately twice the depletion layer thickness. The peak position and relative intensity of all diffraction peaks for the products, Fig. 1b, match standard powder diffraction data (JCPDS 41-1445). The XRD pattern of the hydrothermal treated 8 wt% Sb-SnO_2 thin films exhibit five discreet hkl reflections at 26.6°, 33.9°, 38.0°, 51.8°, and 54.8°, respectively, corresponding to the (110), (101), (200), (211) and (220) crystallographic planes of tetragonal SnO_2 in accordance with the synthetic cassiterite, as shown in ESI, Fig. S3. No characteristic peaks belonging to other SnO_2 crystals or impurities were detected. All diffraction peaks became stronger and sharper with the 400°C and 600°C heat treatments. The average crystalline grain size (D) calculated from the full width at half-maximum, FWHM, of the (110) reflection line using the Scherrer formula, $D = k\lambda/FWHM$, where $k = 0.9$ and $\lambda = 0.15406$ nm, is 2.3 nm for the hydrothermal treated film, 3.8 nm for the 400°C annealed film, and 5.2 nm for the 600°C annealed film. According to the grain control model, the sensor response increase dramatically when the particle size of sensing materials is comparable to or less than two times of Debye length(L_D is about 3nm for SnO_2) [42]. Therefore, the hydrothermal treated and 600°C annealed Sb-SnO_2 films exhibiting an average grain size of about 5 nm are able to achieve rapid transduction of surface interactions into measurable conductance changes [43].

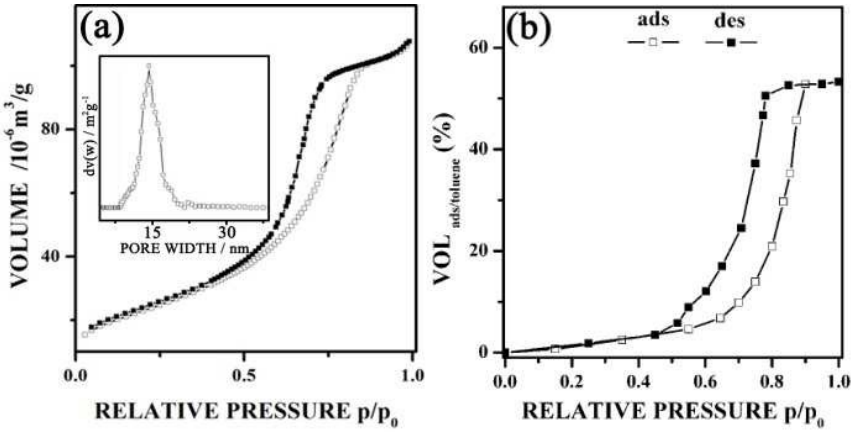

Fig. 2. (a) N_2 adsorption/desorption isotherms and corresponding pore-size distribution (inset of a) for nanoporous 8wt% Sb-SnO_2 thin films after 600°C anneal. (b) Toluene adsorption/desorption isotherm obtained using ellipsometricporosimetry for nanoporous 8wt% Sb-SnO_2 thin films after 600°C anneal.

The porosity and pore size of the 600°C annealed 8wt% Sb-SnO_2 thin films were analyzed using nitrogen adsorption/desorption isotherms (Autosorb-1, Quantachrome Instruments). The data of Fig.2a exhibits a behavior typical of *type IV* isotherms reflecting the presence of an ordered nanoporous structure. The Brunauer-Emmett-Teller (BET) calculated surface area is about 127.8 m^2g^{-1}, with a pore size estimated using Non-local Density Functional Theory (NLDFT) of about 13.5 nm. We also applied ellipsometric porosimetry (Woollam VASE M2000-D) to films prepared on silicon wafers. This method is based on spectroscopic ellipsometry measurements during adsorption/condensation of a

solvent, in our case toluene, in the nanopores which thereby change its refractive index. As shown in Fig. 2b, the toluene adsorption/desorption isotherms of the 600°C annealed Sb-SnO_2 thin film also exhibit a response typical of *type IV* isotherms. The well-defined isotherms indicate a uniformly ordered nanoporous structure, with a measured pore volume of 53.32% at a relative partial pressure of one. Nanoporous gas-sensing materials with high specific surface area and porosity allow for rapid gas diffusion and charge transport and thus rapid sensor response. Thus, it is reasonable to believe that the obtained nanoporous 8wt% Sb-SnO_2 thin films with as high as 127.8 m^2g^{-1} surface area and 53.32% porosity would have enhanced gas-sensing performance.

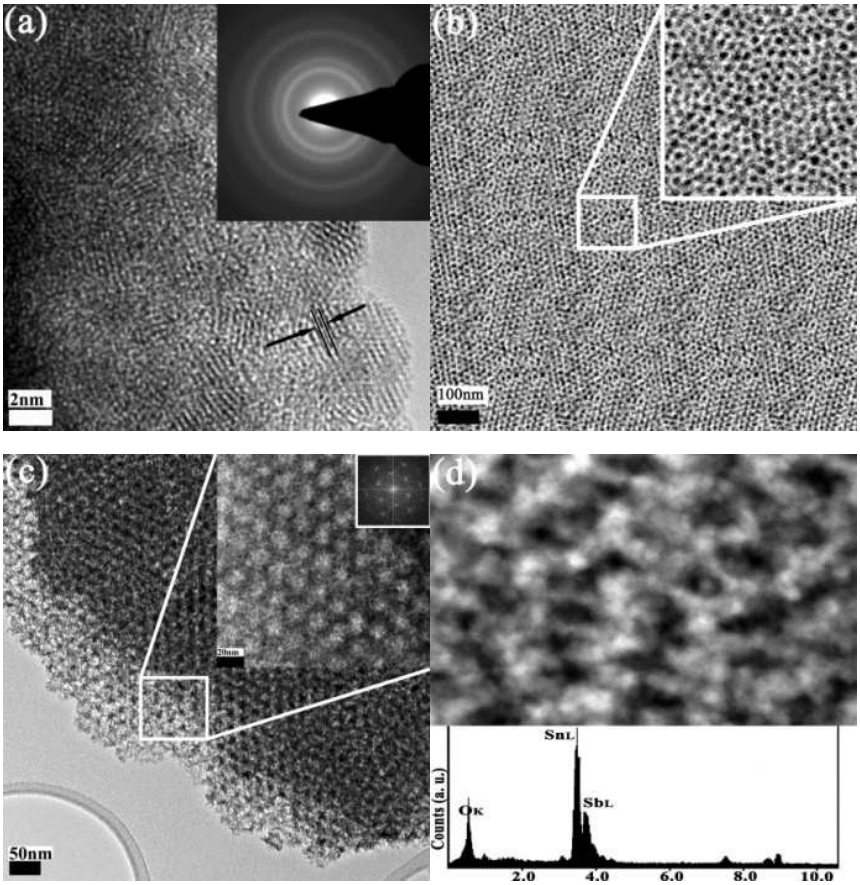

Fig. 3. (a) HRTEM image of SnO_2 thin film after 120°C water vapor hydrothermal treatment. The inset shows SAED pattern of displayed area indicating the polycrystalline nature of the film. (b) FESEM images of a 600°C annealed nanoporous film. (c) TEM image of highly nanoporous 8wt% Sb-SnO_2 thin films annealed at 600°C. The inset is the Fourier transform of the rectangular marked region. (d)STEM image of film cross-section, and EDX pattern of 600°C annealed 8wt% Sb-SnO_2 thin film.

As shown in Fig. 3a, a high resolution transmission electron microscope image of a hydrothermal treated thin film provides important information of highly crystalline nanocrystals. The selected area electron diffraction (SAED) pattern (inset of Fig. 3a) displaying clear diffraction rings indicates that the SnO_2 framework is fully crystallized at the 120°C processing temperature. Fig. 3b shows a field emission scanning electron microscope (FESEM) image of a 600°C annealed nanoporous film. Fig. 3c shows a TEM image of a 600°C annealed nanoporous film，where the nanopore arrays are packed in an ordered arrangement with an average pore size of approximately 13-14 nm. A fast Fourier transformation of the film, the region enclosed within the square depicted in Fig. 3c, indicated

orthorhombic symmetry of a [111] oriented F*mmm* nanostructure [44]. Further information on the nanostructure of the thin film is provided by high resolution TEM (HRTEM) as shown in ESI, Fig.S4. It can be observed that the 600°C annealed nanoporous film is only composed of highly crystalline nanoparticles of cassiterite type, which is in good agreement with the wide-angle XRD studies (Fig. 1b). STEM images, in high-angle annular dark-field mode, travelling over film cross-sections, Fig. 3d, reveal uniform dispersion of the antimony within the ordered nanoporous films. No distinct or pure antimony oxide particles are detected. The result is confirmed by the energy dispersive X-ray scattering (EDX, TITAN 80-300 operating at 300 kV), Fig. 3d, which reveals the presence of antimony and tin, but it is impossible to distinguish antimony from the tin oxide phase, indicating the very good dispersion of antimony over the whole thin film.

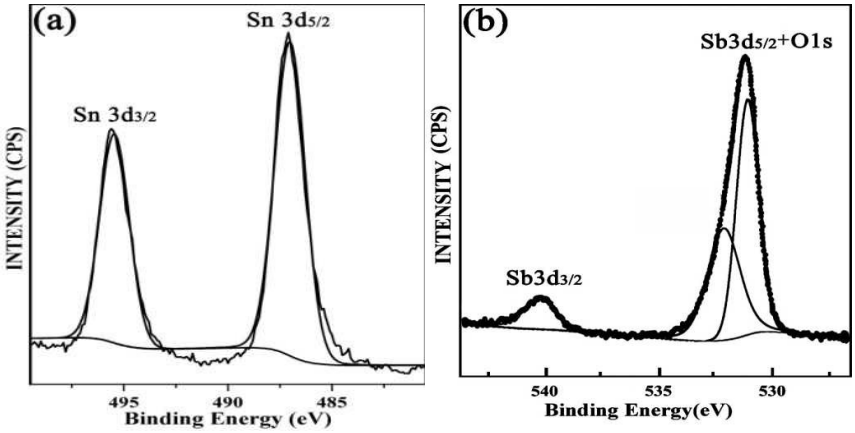

Fig. 4. (a) The high-resolution spectrum of Sn 3d of a 600°C annealed nanoporous Sb-SnO_2 thin film; (b) the high-resolution XPS spectra of superposed Sb $3d_{5/2}$ and Sb $3d_{3/2}$ of a 600°C annealed nanoporous Sb-SnO_2 thin film.

Chemical composition and atomic ratios of Sn, Sb, and O in the Sb doped SnO_2 thin film was analyzed by X-ray photoelectron spectroscopy (XPS, Kratos AXIS Ultra DLD). The XPS analysis demonstrates the existence of Sn, Sb and O without any impurities in the nanoporous Sb-doped SnO_2 thin films. The binding energies at 486.6 and 495.1eV are attributed to Sn $3d_{5/2}$ and $Sn3d_{3/2}$ with a better symmetry, and assigned to the lattice tin in tin oxide, Fig. 4a. The main XPS peaks for oxygen and antimony atoms, O1s and $Sb3d_{5/2}$, are superposed around 531.0eV, as shown in Fig.4b. The $Sb3d_{5/2}$ and $Sb3d_{3/2}$ spin/orbit spectra were assigned to binding energies 531.2eV and 540.1eV [45]. Terrier et al. have developed a method for the measurement of the Sb^{5+}/Sb^{3+} ratio in antimony-doped SnO_2 nanoporous thin film by means of the deconvolution of this Sb $3d_{3/2}$ transition peak [46]. As shown in ESI, Fig. S5, the Sb $3d_{3/2}$ band can be separated into two contributions: the Gaussian line centered at 540.1eV corresponds to antimony with an oxidation state of Sb(V), while the peak at 539.2eV corresponds to Sb(III) [47].

3.2 Application to ethanol sensing

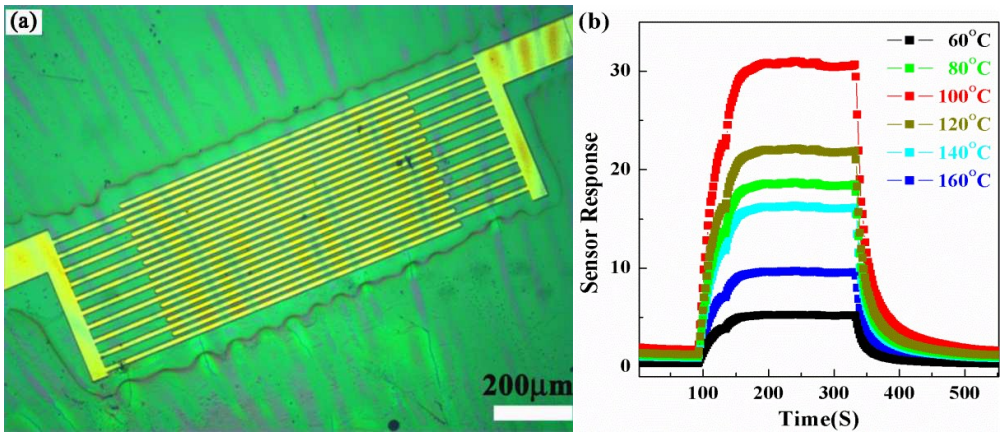

Fig. 5. (a)Microscope image of the interdigital sensor devices with ordered nanoporous Sb doped SnO_2 thin film at room temperature. (b) Response curves of Sb doped SnO_2 sensor exposed to 50ppm ethanol at different operating temperature: 60°C, 80°C, 100°C, 120°C, 140°C, and 160°C, respectively.

Interdigital sensor devices were manufactured by applying standard semiconductor lithography and metallization processes, Fig. 5a. Silicon wafer substrates were employed, with titanium as a binding agent, platinum as a diffusion barrier, and gold as the contact material. The central metal structure consists of twenty fingers. Each finger is 10μm in width and 1mm in length, finger-finger spacing is 8μm, with a finger-to-finger overlap of 800μm. The interdigitated-finger array was spin-coated with the gas responsive Sb-SnO_2 thin films. It is known that nanoporous gas sensing films fabricated by usual approaches and a subsequent annealing normally sustain a dramatic decrease in effective surface area due to nanostructure collapse[21, 22]. Hence to date only a few nanoporous SnO_2-based thin films have been discovered that reveal relatively high sensitivity to low-level concentration of ethanol at low temperature. In contrast, our post-synthetic hydrothermal process allows the subsequently annealed Sb-SnO_2 thin films excellent thermal stability, resulting in highly ordered nanoporous structure of large surface area, small crystal particle size and excellent dispersion of Sb dopant.

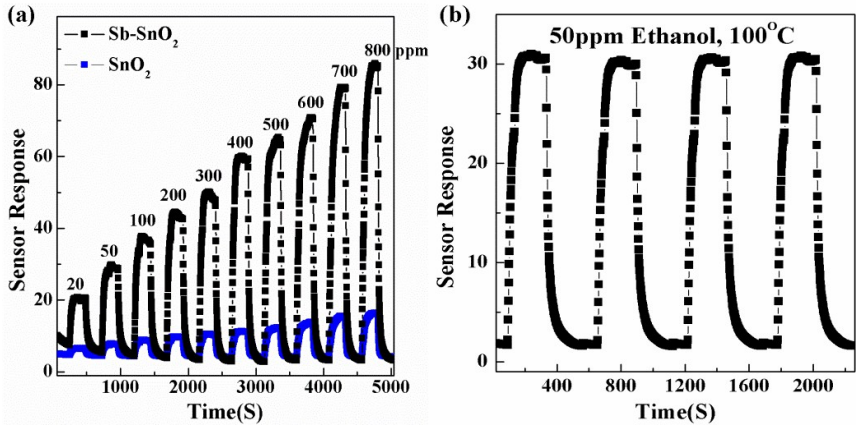

Fig. 6. Gas sensing behavior at low temperature (100°C) of: (a) Nanoporous 8 wt% Sb doped SnO_2 thin film after 600°C anneal. Shown are cyclic response changes when drying air is introduced or removed from a reducing process gas stream (here 20 ppm, 50 ppm, 100 ppm, 200 ppm, 300 ppm, 400 ppm, 500 ppm, 600 ppm, 700 ppm,800 ppm ethanol diluted in nitrogen). (a) Cyclic response changes between air, and 50ppm ethanol in N_2.

The operating temperature strongly influences the adsorption and desorption rates of oxygen ions on the metal-oxide surface, and therefore controls the sensor response. The performance of materials as gas sensor is shown in Fig. 5b after removal of the residual template material through the 600 °C anneal. Ethanol detections with a concentration of 50ppm at different operating temperature were performed to determine the optimum operating temperature, at which the sensor shows a maximum response to ethanol. For a comparative study, the sensor response is defined as $S=R_a/R_g$, where R_a and R_g are the electrical resistances in air and in the presence of the gas, respectively. It is shown that from 60°C to 100°C the response increases with operating temperature and reaches as maximum of 30.8 at 100 °C, and then decreases with further increase in temperature. Therefore, 100°C is deemed as the optimal operating temperature and all other sensing tests are conducted at this temperature.

Concerning sensitivity of nanostructured films, the carrier mobility is enhanced when the nanoparticle size is similar to or less than two times of Debye length (L_D is about 3nm for SnO_2). Then the change in the nanoparticle size influences the conductivity of the whole film [42]. In fact, the number of carriers released during chemisorption is usually related to the EtOH chemistry on the SnO_2 surface by the ionosorption model as reviewed recently [48]:

$$C_2H_5OH+O^- \leftrightarrow CH_3CHO+H_2O+e^- \quad (1)$$

Compared to the pure nanoporous SnO_2 thin film, Sb doped SnO_2 thin film exhibited greatly improved sensitivity. Fig. 6a depicts the reversible sensor response to a reducing gas mixture of 20 ppm, 50 ppm, 100 ppm, 200 ppm, 300 ppm, 400ppm, 500 ppm, 600ppm, 700 ppm, and 800 ppm ethanol diluted in-N_2 and dry air. The ethanol nanosensor containing 8wt% Sb shows recoverable response with minor baseline drift and the response increases with the increasing gas concentration. Evidently, the sensor based on Sb doped SnO_2 sensing film has higher response amplitudes towards each concentration. Furthermore, the response amplitude is highly dependent on ethanol concentration, while the increase in the response amplitude of pure nanoporous SnO_2 sensor is not so remarkable. By keeping the ethanol vapour concentration range of 20ppm-800ppm, the sensitivities of ethanol nanosensors containing 8wt% Sb are about 20.6, 30.8, 36.8, 45.7, 52.9, 59.7, 65.2, 70.6, 78.9 and 85.3, which are much higher than the values of the pure nanoporous SnO_2 sensors. Taking 50ppm ethanol for example, as shown in Fig. 6a, the response of the ethanol nanosensor containing 8wt% Sb to alternating ethanol/N_2 and air atmospheres is both stable and fully reversible, and is about 9.2 times higher than the value of the pure SnO_2 sensor. Above 800 ppm, the response slowly increases, which indicates that the sensor becomes more or less saturated. There were also some reports in the literature on the enhanced sensing performance of sensing materials combined of dopants and semiconductors, as shown in ESI, Table S1. Vaishnav *et al.* achieved the detecting of ethanol vapour at low temperature with low response value (~1.02) by using 17% SnO_2-In_2O_3 film as sensing materials.[49] Neri *et al.* improved the sensing response value to about 5, applying In doped SnO_2 nanopowders exposed to 100 ppm ethanol vapour at 150 °C, but the response and recovery time were nearly 1000 sec.[50] Naghadeh *et al.* synthesized 0.05 wt% MWCNTs/SnO_2 nanocomposites as ethanol sensing materials. The sensitivity was increased and the response time was decreased, but the recovery time was still more than 300 sec.[51] Ma *et al.* fabricated porous Zn doped SnO_2 hollow nanospheres as ethanol gas sensor, and got better sensitivity to 50 ppm ethanol. The specified response and recovery time were not shown in the literature.[52] Further increase of the sensitivity was owing to the use of SnO_2/TiO_2 nanobelts based gas sensor, and the response value was 18.5 upon to 100 ppm ethanol. However, both response time and

recovery time were more than 200 sec.[53] In this work, the highly ordered Sb doped SnO_2 sensing films exhibit fast response upon ethanol exposure within 54 sec and they are fully recoverable upon gas release within 58 sec; these sensors show repeatable performance with minor baseline drift upon multiple cycles of 50ppm of ethanol vapour exposure and release as shown in Fig. 6b. A similar sensitivity could not be observed in case of a nanoporous tin dioxide thin film prepared under similar conditions just without antimony.

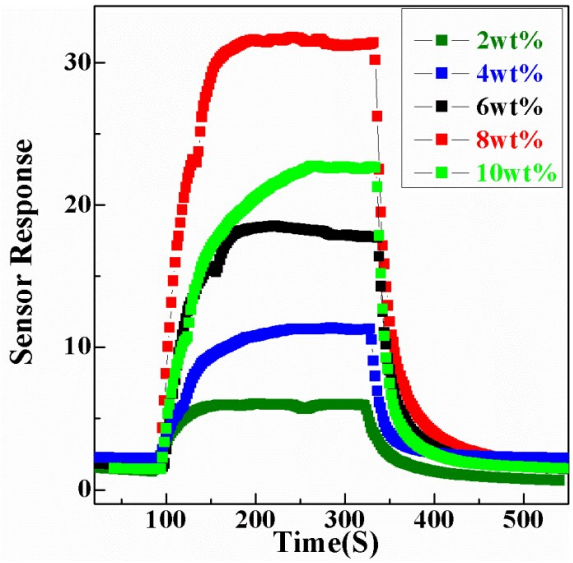

Fig. 7. Response curves of sensing films with different Sb doping contents ranging from 2wt% to 10wt% to 50 ppm ethanol at 100°C.

In order to quantify the effect of Sb on the gas response, the response behaviours of sensing films with different concentration of Sb are shown in Fig. 7. As the concentration of Sb increases from 2wt% to 8wt%, the response to 50 ppm ethanol vapor also increases gradually. The response values to ethanol vapor for sensing films with Sb doping content at 2wt%, 4wt%, 6wt% and 8wt% are 6.1, 11.3, 18.2 and 30.8, respectively. A further increase in the Sb concentration decreases the response value to 22.6 resulting in an optimal Sb doping content at 8wt%. At the optimal antimony doping level of 8 wt %, Sb-doped SnO_2 thin film exhibits not only high response but also high ethanol selectivity against acetone and other gases at the gas concentration of 50 ppm. It is crucial to note that the highest response to ethanol of 8wt% Sb-doped SnO_2 based sensors is possibly attributed to the difference in the interaction between target gas molecules and the surface of sensor materials. At the measured temperature, the pre-adsorbed oxygen on the surface of sensing material prefer to interact with ethanol.[54] Therefore, when being exposed to ethanol, lots of free electrons were released back to the sensing layer, leading to a large resistance change. As a result, the 8wt% Sb-doped SnO_2 based sensors show the highest sensitivity to ethanol. At higher Sb doping levels (10wt%), the ethanol response reduces substantially compared with the optimally doped one. The disadvantageous traits may be due to the high-level surface disorder on sensing film surfaces induced by the heavy Sb doping. The surface disorder can be exhibited as defective surface states that trap charge carries, causing pinning of Fermi-level, less change of surface conductivity due to charge transfer from reducing reaction and deteriorated gas response.[55] However, more in-depth studies are necessary to investigate the sensitive

behaviour of such ordered nanoporous sensing films to ethanol among many VOCs.

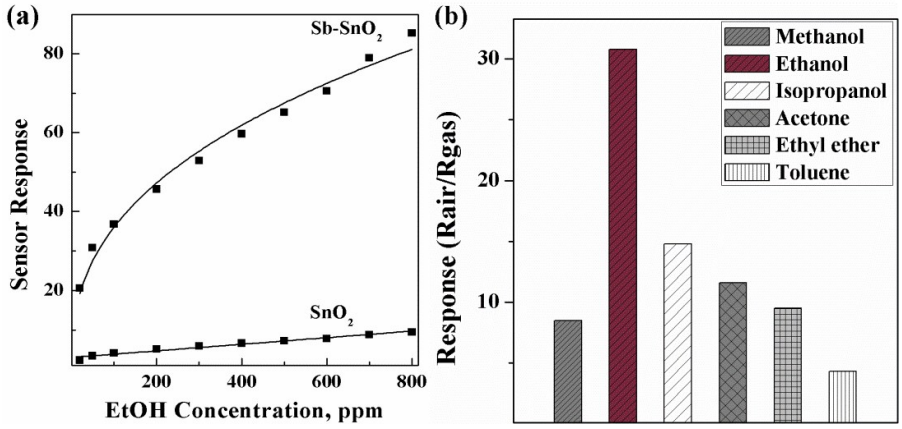

Fig. 8. (a) The power law fitting of sensor response on ethanol concentration of ordered nanoporous Sb doped SnO_2 thin film and pure SnO_2 thin film. (b) The selectivity of ordered nanoporous Sb doped SnO_2 thin film toward methanol, ethanol, isopropanol, acetone, ethyl ether, toluene at 100°C, respectively.

In Fig. 8a, the highly ordered Sb doped SnO_2 based gas sensors show a power law relationship between the sensor response (S) and gas concentration (C_{EtOH}), and the correlation coefficient (n) was estimated to be 0.391 within the gas concentration ranging from 20 to 800ppm. High correlation coefficients are necessary for high sensitivity. They are determined by nanoporous structure which strongly influences carrier mobility in the sensing film.

$$S = a \cdot C_{EtOH}^{n}$$

Selectivity is another key parameter for gas sensors. Fig. 8b shows the bar diagram of device response to different target gases (50ppm) at 100°C. The sensors exhibit high response to ethanol vapour and negligible response to isopropanol, acetone, ethyl ether and toluene. As show in Fig. 8b, the sensor shows the highest response to ethanol with the value of up to 30.8, which for other gases the response is not higher than 15. That is to say, the present sensor displays quite outstanding selectivity to ethanol, especially the Sb-doped SnO_2, of which the responses reach 8.5, 14.8, 11.6, 9.5, and 4.3 to methanol, isopropanol, acetone, ethyl ether, and toluene, respectively.

According to the well-known mechanism of n-type semiconductor gas sensors, the gas-sensing property depends on the redox reaction between reducing gas and chemisorbed oxygen adsorbates (O^{2-}, O^{-} and O^{2-} depending on the operating temperature) on the surface of nanoporous SnO_2 thin film, resulting in the re-injection of electrons into the thin film, thus induces an abrupt resistance change of the metal oxide and then presents response. In this work, the good ethanol-sensing performance of the SnO_2 thin film doped with 8 wt% Sb, particularly the high response and low operating temperature, is explained from the important aspect of small grain size, ordered nanoporous structure, and high surface area. Firstly, small grain size (D~5.2nm) of the nanocrystal subunits and the three-dimensional interconnected nanoporous structure are responsible for the dramatically improved electrochemical properties of SnO_2 thin films[56]. Sb doping further increases the sensor response due to the electrical sensitization effects of Sb_2O_3 and Sb_2O_5. The optimization of the synthesis parameters and the conditions of post-synthetic hydrothermal treatments lead to materials differing significantly in the

physicochemical properties and their sensing behaviour. On the other hand, for the 8wt% Sb-doped SnO_2 based nanoporous sensing films with ordered pores nanostructure serving as diffusion channels, the response-recovery process is probably quickened due to the enhanced gas diffusion and the sensor response is probably increased because of the formation of conjugated electron depletion layers on both the outer and inner surfaces. The high surface area of the thin film (127.8 m^2g^{-1}) makes the adsorption of ethanol molecules on the surface of our sensors easy. The ordered two dimensional structure of the nanoporous films can facilitate fast mass transfer of the ethanol molecules to and from the interaction region as well as improve the rate for charge carriers to transverse the barriers induced by molecular recognition along the nanoporous films [52, 57, 58].

4. Conclusions

In summary, based on a cost-effective, low-temperature and environment-friendly synthetic process, highly ordered and homogeneous nanoporous thin films of antimony doped tin dioxide have been fabricated from a 120°C water vapor hydrothermal treatment. Gas sensing thin films depict ordered nanostructures maintained at temperatures up to 600 °C in combination with highly crystalline tin oxide of cassiterite structure, outstanding nanostructure, and long-term thermal stability. The highly ordered thin films feature in stable nanoporous texture; small grain size and high surface area make them the promising candidates in preparing highly sensitive gas sensors. The best gas sensing result, a change of ~ 30 times of electrical resistance in response to 50 ppm ethanol at 100°C, was obtained in the SnO_2 thin film doped with 8 wt% Sb. The novel synthesis route is potentially applicable for preparing high quality ordered nanoporous crystalline materials for applications including gas sensing, photocatalysis and 3rd generation photovoltaics.

5. Acknowledgments

This work was supported by the Startup Foundation for Introducing Talent of NUIST and the grant of Specially-Appointed Professor of Jiangsu. We thank the Siemens AG for the helping in the design, preparation and donation of the sensor devices. We thank the University of Munich and especially Prof. Dr. T. Bein for his constant support.

References:

1. Z.-H. Lin, Y. Xie, Y. Yang, S. Wang, G. Zhu and Z. L. Wang, *ACS Nano*, 2013, **7**, 4554.
2. X. Wang, Y. Wang, D. Aberg, P. Erhart, N. Misra, A. Noy, A. V. Hamza and J. Yang, *Adv. Mater.* , 2011, **23**, 117.
3. J. Du, D. Liang, H. Tang and X. P. A. Gao, *Nano Lett.* , 2009, **9**, 4348.
4. B. Li and D. N. Lambeth, *Nano Lett.* , 2008, **8**, 3563.
5. J.-H. Lee, *Sensors and Actuators B*, 2009, **140**, 319.
6. N. S. Ramgir, Y. Yang and M. Zacharias, *Small*, 2010, **6**, 1705.
7. F. Gu, L. Zhang, X. Yin and L. Tong, *Nano Lett.* , 2008, **8**, 2757.
8. B. Li, G. Sauve, M. C. Iovu, M. Jeffries-EL, R. Zhang, J. Cooper, S. Santhanam, L. Schultz, J. C. Revelli, A. G. Kusne, T. Kowalewski, J. L. Snyder, L. E. Weiss, G. K. Fedder, R. D. McCullough and D. N. Lambeth, *Nano Lett.* , 2006, **6**, 1598.
9. J. T. Robinson, F. K. Perkins, E. S. Snow, Z. Wei and P. E. Sheehan, *Nano Lett.* , 2008, **8**, 3137.
10. T. Brezesinski, A. Fischer, K.-i. Iimura, C. Sanchez, D. Grosso, M. Antonietti and B. M. Smarsly, *Adv. Funct. Mater.* , 2006, **16**, 1433.
11. S. Y. Choi, B. Lee, D. B. Carew, M. Mamak, F. C. Peiris, S. Speakman, N. Chopra and G. A. Ozin, *Adv. Funct. Mater.* , 2006, **16**, 1731.
12. A. Tricoli, M. Righettoni and A. Teleki, *Angew Chem Int Ed Engl*, 2010, **49**, 7632.
13. J. N. Kondo and K. Domen, *Chem. Mater.* , 2008, **20**, 835.
14. M. Tiemann, *Chem. Eur. J.* , 2007, **13**, 8376.
15. X. Gou, G. Wang, X. Kong, D. Wexler, J. Horvat, J. Yang and J. Park, *Chem. Eur. J.* , 2008, **14**, 5996.
16. L. Jia and W. Cai, *Adv. Funct. Mater.* , 2010, **20**, 3765.
17. Q. Cao and J. A. Rogers, *Adv. Mater.* , 2009, **21**, 29.
18. M. H. Huang, Y. Wu, H. Feick, N. Tran, E. Weber and P. Yang, *Adv. Mater.* , 2001, **13**, 113.
19. Y. S. Jung, W. Jung, H. L. Tuller and C. A. Ross, *Nano Lett.* , 2008, **8**, 3776.
20. Y. Kuang, G. Chen, X. Lei, L. Luo and X. Sun, *Sens. Actuators, B* 2013, **181**, 629.
21. A. Rosental, A. Tarre, A. Gerst, T. Uustare and V. Sammelselg, *Sens. Actuators, B* 2001, **77**, 297.
22. N. Rajesh, J. C. Kannan, T. Krishnakumar, S. G. Leonardi and G. Neri, *Sens. Actuators, B* 2014, **194**, 96.
23. R.-J. Wu, D.-J. Lin, M.-R. Yu, M. H. Chen and H.-F. Lai, *Sens. Actuators, B* 2013, **178**, 185.
24. Z. Jin, H.-J. Zhou, Z.-L. Jin, R. F. Savinell and C.-C. Liu, *Sens. Actuators, B* 1998, **52**, 188.
25. E. Strelcov, Y. Lilach and A. Kolmakov, *Nano Lett.* , 2009, **9**, 2322.
26. V. V. Sysoev, J. Goschnick, T. Schneider, E. Strelcov and A. Kolmakov, *Nano Lett.* , 2007, **7**, 3182.
27. D. Zhang, Z. Liu, C. Li, T. Tang, X. Liu, S. Han, B. Lei and C. Zhou, *Nano Lett.* , 2004, **4**, 1919.
28. X. D. Wang and O. S. Wolfbeis, *Anal. Chem.* , 2013, **85**, 487.
29. X. D. Wang and O. S. Wolfbeis, *Anal. Chem.* , 2016, **88**, 203.
30. C. Marichy, N. Donato, M.-G. Willinger, M. Latino, D. Karpinsky, S.-H. Yu, G. Neri and N. Pinna, *Adv. Funct. Mater.* , 2011, **21**, 658.
31. Y. E. Chang, D. Y. Youn, G. Ankonina, D. J. Yang, H. G. Kim, A. Rothschild and I. D. Kim, *Chem Commun (Camb)*, 2009, 4019.
32. Y. Wang, X. Jiang and Y. Xia, *J. Am. Chem. Soc.* , 2003, **125**, 16176.
33. R. Ab Kadir, Z. Li, A. Z. Sadek, R. Abdul Rani, A. S. Zoolfakar, M. R. Field, J. Z. Ou, A. F. Chrimes and K. Kalantar-zadeh, *J. Phys. Chem. C* 2014, **118**, 3129.
34. N. Van Hieu, H.-R. Kim, B.-K. Ju and J.-H. Lee, *Sens. Actuators, B* 2008, **133**, 228.
35. J.-H. Park and J.-H. Lee, *Sens. Actuators, B* 2009, **136**, 151.

36. A. Zima, A. Köck and T. Maier, *Microelectron. Eng.* , 2010, **87**, 1467.
37. Y. D. Wang, I. Djerdj, M. Antonietti and B. Smarsly, *Small*, 2008, **4**, 1656.
38. S. Shao, X. Qiu, D. He, R. Koehn, N. Guan, X. Lu, N. Bao and C. A. Grimes, *Nanoscale*, 2011, **3**, 4283.
39. H. Miyata, M. Itoh, M. Watanabe and T. Noma, *Chem. Mater.* , 2003, **15**, 1334.
40. V. N. Urade and H. W. Hillhouse, *J. Phys. Chem. B*, 2005, **109**, 10538.
41. J. H. Pan, S. Y. Chai, C. Lee, S.-E. Park and W. I. Lee, *J. Phys. Chem. C*, 2007, **111**, 5582.
42. H. Ogawa, M. Nishikawa and A. Abe, *J. Appl. Phys.* , 1982, **53**, 4448.
43. A. Rothschild and Y. Komem, *J. Appl. Phys.* , 2004, **95**, 6374.
44. C. Boissiere, D. Grosso, S. Lepoutre, L. Nicole, A. B. Bruneau and C. Sanchez, *Langmuir*, 2005, **21**, 12362.
45. D. Doblera, S. Oswalda, J. Wernera, W. Arabczykb, G. Behra and K. Wetziga, *Chem. Phys.* , 2003, **286**, 375.
46. C. Terrier, J. P. ; Chatelon, J. A. Roger, R. Berjoan and C. Dubois, *J. Sol-Gel Sci. Technol.* , 1997, **10**, 75.
47. C. Terrier, J. P. Chatelon, R. Berjoan and J. A. Roger, *Thin Solid Films* 1995, **263**, 37.
48. A. Gurlo, *ChemPhysChem*, 2006, **7**, 2041.
49. V. S. Vaishnav, P. D. Patel and N. G. Patel, *Thin Solid Films* 2005, **490**, 94.
50. G. Neri, A. Bonavita, G. Micali, G. Rizzo, N. Pinna, M. Niederberger and J. Ba, *Sens. Actuators B* 2008, **130**, 222.
51. S. B. Naghadeh, S. Vahdatifar, Y. Mortazavi, A. A. Khodadadi and A. Abbasi, *Sens. Actuators, B* 2016, **223**, 252.
52. X. Ma, H. Song and C. Guan, *Sens. Actuators, B* 2013, **188**, 193.
53. G. Chen, S. Ji, H. Li, X. Kang, S. Chang, Y. Wang, G. Yu, J. Lu, J. Claverie, Y. Sang and H. Liu, *ACS Appl. Mat. Interfaces* 2015, **7**, 24950.
54. K.-M. Li, Y.-J. Li, M.-Y. Lu, C.-I. Kuo and L.-J. Chen, *Adv. Funct. Mater.* , 2009, **2009**, 2453.
55. G. Korotcenkov, I. Boris, V. Brinzari, S. H. Han and B. K. Cho, *Sens. Actuators, B*, 2013, **182**, 112.
56. C. Xu, J. Tamaki, N. Miura and N. Yamazoe, *Sensors and Actuators B*, 1991, **3**, 147.
57. Y. Kwon, H. Kim, S. Lee, I.-J. Chin, T.-Y. Seong, W. I. Lee and C. Lee, *Sens. Actuators, B* 2012, **173**, 441.
58. L. Zhang and Y. Yin, *Sens. Actuators, B* 2013, **185**, 594.

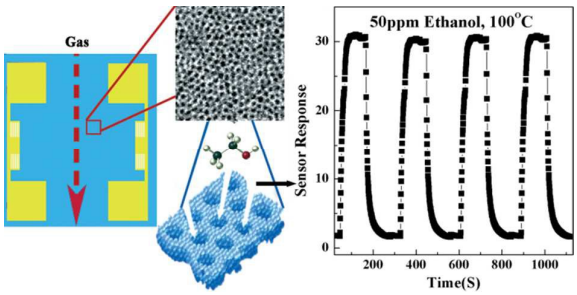

Highly ordered nanoporous Sb-SnO_2 sensing films synthesized through psHT treatment present high sensitivity to 50 ppm ethanol at low temperature.